ChemBioChem

Research Article
doi.org/10.1002/cbic.202300773

Chemistry Europe
European Chemical Societies Publishing

www.chembiochem.org

Investigating Protein Binding with the Isothermal Ligand-induced Resolubilization Assay

Riley A. Prout-Holm,[a] Cerissa C. van Walstijn,[b] Alana Hitsman,[a] Michael J. Rowley,[a] Jonas E. Olsen,[a] Brent D. G. Page,*[a] and Adam Frankel*[a]

Target engagement assays typically detect and quantify the direct physical interaction of a protein of interest and its ligand through stability changes upon ligand binding. Commonly used target engagement methods detect ligand-induced stability by subjecting samples to thermal or proteolytic stress. Here we describe a new variation to these approaches called Isothermal Ligand-induced Resolubilization Assay (ILIRA), which utilizes lyotropic solubility stress to measure ligand binding through changes in target protein solubility. We identified distinct buffer systems and salt concentrations that compromised protein solubility for four diverse proteins: dihydrofolate reductase (DHFR), nucleoside diphosphate-linked moiety X motif 5 (NUDT5), poly [ADP-ribose] polymerase 1 (PARP1), and protein arginine *N*-methyltransferase 1 (PRMT1). Ligand-induced solubility rescue was demonstrated for these proteins, suggesting that ILIRA can be used as an additional target engagement technique. Differences in ligand-induced protein solubility were assessed by Coomassie blue staining for SDS-PAGE and dot blot, as well as by NanoOrange, Thioflavin T, and Proteostat fluorescence, thus offering flexibility for readout and assay throughput.

Introduction

The formation of noncovalent interactions between ligand and protein, as well as the solvation effects associated with ligand binding, make protein-ligand complexation an energetically favourable process with both enthalpic and entropic contributions to binding. This process, as Koshland pointed out in 1958, can induce to some degree a structural adjustment within the protein to fit the ligand.[1] According to Le Chatelier's principle, the introduction of a ligand establishes a new equilbrium between folded unliganded (F) and folded ligand-bound protein (FL), thus causing a shift in its overall equilibrium (U ↔ F ↔ FL) in favour of a stable FL population over the unfolded population (U).[2–5] Even during the course of protein folding, ligands can serve a chemical chaperone role, facilitating the stabilization of early folding intermediates through to quaternary structures and resulting in the formation of functional proteins.[6–8]

The use of thermal stress to measure ligand-induced stability for purified proteins has been developed into well-established binding and target engagement assays such as Differential Scanning Fluorimetry (DSF)[9] and the protein thermal shift assay (PTSA).[10] In these assays, the increase in heat causes proteins to unfold, inducing protein aggregation at higher temperatures. Measuring protein aggregation over a range of temperatures can produce an aggregation curve that can be used to derive an aggregation or melting temperature (T_{agg} or T_m, respectively). One can then investigate how these curves or values shift in the presence of experimental compounds to determine if ligand binding is occurring. The drug affinity responsive target stability (DARTS) assay is an alternative target engagement method that measures proteolytic stability rather than thermal stability.[11] This assay utilizes an exogenous protease to degrade a protein of interest in the presence or absence of ligands. The protein contents are then analyzed by gel electrophoresis and differences in quantitated band intensities between unliganded and ligand-protected samples can indicate target engagement. Both heat-based and proteolytic resistance-based assays are highly valuable tools for drug discovery and development, allowing scientists to determine if experimental compounds can bind the intended target(s) in biological settings.

Proteins are susceptible to other forms of physical stressors that can affect their stability, such as the buffer system, pH, salt, and co-solvents like DMSO and glycerol.[12,13] The effect of salt ions on protein solubility is well documented with much of the focus on the lyotropic behavior of different ions. This behavior can go one of two ways for proteins: "salting in" occurs when a high concentration of an ion improves protein solubility, and "salting out" occurs when a high concentration of an ion drives

[a] R. A. Prout-Holm, A. Hitsman, M. J. Rowley, J. E. Olsen, Prof. B. D. G. Page, Prof. A. Frankel
Faculty of Pharmaceutical Sciences
The University of British Columbia
2405 Wesbrook Mall, Vancouver, BC V6T 1Z3 (Canada)
E-mail: brent.page@ubc.ca
adam.frankel@ubc.ca

[b] C. C. van Walstijn
Faculty of Science
Utrecht University
Heidelberglaan 8, 3584 CS, Utrecht (The Netherlands)

Supporting information for this article is available on the WWW under https://doi.org/10.1002/cbic.202300773

the protein into an insoluble precipitate.[14] These salt-derived protein solubility effects often arise through ion-induced changes in surface charge density, net charge, hydration shell size, and polarizability.[14–17] Buffer-induced stress can also perturb protein stability as buffer ions can interact with protein surfaces to modify surface charge density and hydrophobicity.[15] These perturbations in surface ion topography can impart a significant degree of electrostatic stress on proteins, ultimately leading to changes in protein folding and solubility.[14–17]

To improve protein purification, structure determination, and protein functionality, a range of buffers are routinely explored with different pH levels, salts and salt concentrations, and/or co-solvents in arrayed formats.[12,13,18–24] We have herein utilized the same underlying principles to identify buffer conditions that promoted protein aggregation for four purified human target proteins: dihydrofolate reductase (DHFR), Nudix-type hydrolase 5 (NUDT5), the catalytic domain of poly [ADP-ribose] polymerase 1 (PARP1cd; amino acids 661–1014), and protein arginine *N*-methyltransferase 1 (PRMT1). We identified destabilizing conditions from a small array of buffers and salt concentrations. Brief exposure to these conditions at ambient or near-physiological temperatures facilitated protein aggregation. In the presence of target-specific ligands, however, protein solubility was maintained or "rescued" from their unliganded fate. The resistance to this solubility stress forms the basis of our new screening method termed Isothermal Ligand-induced Resolubilization Assay (ILIRA). This assay allows for rapid target engagement screening without the need for specialized equipment or resources.

Results and Discussion

Establishing a salt and buffer screening array

We hypothesized that the cumulative effects of salt- and buffer-derived protein solubility stress could be used, at a constant temperature (below the T_m value for a given target protein), as an alternative stress method to detect and quantify ligand binding. To find these conditions for each of the four proteins (Scheme 1), we subjected purified proteins to an array of buffer conditions at pH 7.4, including 10 mM phosphate buffer (PB), HEPES, Tris, or water (containing dilute protein storage buffer). These conditions were combined with different salt concentrations consisting of either 0, 10, or 100 mM NaCl. It is important to note that each purified target protein was in a corresponding storage buffer (noted in the Experimental Section), which was diluted but not removed during the assay process. Dilution factors of storage buffer components were as follows based on the volume of pure target protein added to the ILIRA samples: 50-fold for PARP1cd and DHFR, 33-fold for PRMT1, and 20-fold for NUDT5. After a 30-min incubation, samples were centrifuged to separate the soluble protein fraction from any precipitate that may have formed, and soluble proteins were then resolved by gel electrophoresis.

With the aforementioned proteins of interest, 2 μg of protein per sample allowed for facile visualization with Coomassie staining on a gel and provided enough material to facilitate precipitation under solubility stress conditions. These conditions resulted in decreased densitometric signal quench of soluble protein. Each of the four proteins required distinct constant temperatures during the incubation phase in order to elicit solubility stress among the conditions tested given inherent differences in protein stability. In previous thermal shift assays in cells with DHFR, NUDT5, and PARP1, T_{agg} values were measured at 41.5 °C,[25] 76–80 °C,[26] and 48 °C,[27] respectively. Our group previously determined 52.4 °C as the T_m of PRMT1 *via* DSF.[28] The temperatures required to destabilize these proteins in the salt and buffer array (Figure 1) fell below what is required to thermally stress these proteins. DHFR was readily destabilized at 22 °C (ambient temperature) in all buffers regardless of NaCl concentration. Notably, NUDT5 required an incubation only at 42 °C in water and 100 mM NaCl to achieve solubility stress, which is remarkable considering NUDT5's thermal stability.[26] PRMT1 and PARP1cd both displayed variable solubility stress at 37 °C in all buffers and NaCl concentrations. From the results in Figure 1, we were then able to select ILIRA salt and buffer conditions. We chose conditions so that quenched sample band intensities could still be readily quantitated by densitometry (some solubility stress conditions provided a greater signal quench than the ones chosen): DHFR in water and no salt (22 °C), NUDT5 in water with 100 mM NaCl (42 °C), PARP1cd in 10 mM PB with 100 mM NaCl (37 °C), and PRMT1 in water with 100 mM NaCl (37 °C).

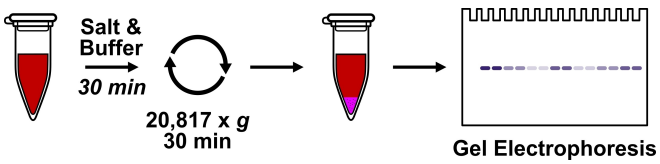

Scheme 1. ILIRA workflow.

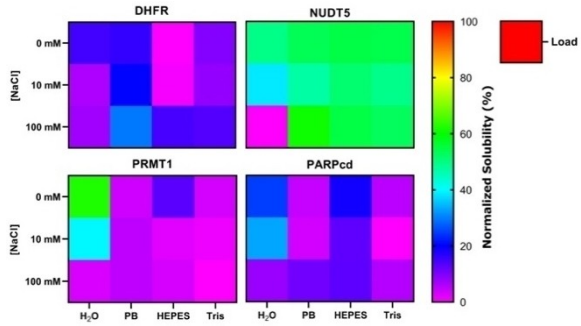

Figure 1. Salt and buffer array heat maps of four target proteins. Proteins were incubated in an array of salt and buffer conditions as indicated prior to quantitation of soluble fractions. Band intensities from Coomassie-stained PAGE gels were normalized to the initial protein load and presented as a heat map prepared in GraphPad Prism 9.3.1.

DHFR

Human DHFR is a 21.5-kDa enzyme that reduces folate using the NADPH cofactor first to dihydrofolate (DHF) and then tetrahydrofolate (THF), a key molecule in one-carbon metabolism needed for cell growth and proliferation by facilitating *de novo* synthesis of DNA precursors and amino acids.[29] Small-molecule inhibitors of DHFR targeting a diverse range of diseases include methotrexate, trimethoprim, and pyrimethamine (Pyr).[25,30] The latter compound was chosen to demonstrate ligand binding to DHFR using ILIRA.

In Figure 2A, we show that the ILIRA rescue of protein signal is specific to DHFR binding to its ligand (Pyr), as the other small molecule (EPZ015666; a PRMT5 inhibitor, employed as the negative control (Neg)) failed to provide any protein stabilizing effect at the same concentration. This result demonstrates a ligand-specific effect in solublity rescue. Furthermore, Pyr showed a dose-dependent rescue of the DHFR quench, beginning as low as 1–10 μM Pyr and saturating at concentrations ≥ 50 μM Pyr (Figure 2B). The Pyr IC_{50} against DHFR was recently determined to be 16.9 μM in an enzymatic assay that included NADPH and the competitive substrate DHF,[25] which falls within the range of the ILIRA results. Interestingly, ILIRA revealed the stabilizing interaction between DHFR and Pyr in the absence of NADPH, perhaps reflecting the random order of ligand binding between cofactor and substrate seen for DHFR from a thermophilic organism at 20 °C.[31]

NUDT5

Human NUDT5 is a 24.3-kDa ADP-sugar pyrophosphatase whose function is to control intracellular ADP-ribose levels.[32] Its implication in nuclear ATP production, chromatin remodeling in breast cancer cells, and poor prognosis for breast cancer patients make NUDT5 an attractive therapeutic target.[33] TH5427 is a small molecule inhibitor of NUDT5 (IC_{50} = 29 nM) shown to decrease nuclear ATP production, hormone-responsive gene expression, and cell proliferation in breast cancer cell lines.[26,34] This compound showed significant stabilization of NUDT5 in thermal stability and DARTS assays,[26] suggesting that it would be a good candidate for ILIRA with NUDT5.

Similar to the dose-response observed for DHFR and Pyr, NUDT5 exhibited a solubility rescue in the presence of TH5427 (Figure 3). However, given tight binding between ligand and target, even 1 μM TH5427 resulted in a near saturation of the dose-response curve, similar to the stabilizing effects TH5427 elicited for NUDT5 in the previously reported thermal stability and DARTS assays.[26] Both the vehicle-only and negative controls did not produce responses comparable to TH5427 (Figure 3).

PARP1cd

Human PARP1 is a multi-domain, 113-kDa protein that transfers ADP ribosyl groups from NAD^+ to acceptor chromatin and chromatin-associated proteins, and mediates base excision repair in DNA single-strand breaks.[35] Given its role in DNA repair processes, PARP1 is an attractive target as part of combination therapy for many cancers.[36] For the purpose of this proof-of-concept study, only its 39.6-kDa catalytic domain was used to test Olaparib response in ILIRA. Olaparib is a small molecule PARP1 inhibitor with a reported IC_{50} of 5 nM that competes against NAD^+ for binding in the catalytic domain.[37,38]

PARP1cd responded to solubility stress and rescue by Olaparib as predicted (Figure 4). While the quench condition resulted in a low level of soluble PARP1cd similar to that of the vehicle-only control, the negative control of 100 μM Pyr appeared to destabilize the protein even further. At concentrations of Olaparib between 1–100 μM, the ILIRA effect plateaued at the lowest concentration tested, which is consistent with its high affinity for PARP1cd.[37]

PRMT1

Human PRMT1(v1)[39] is a 40.5-kDa methyltransferase that transfers methyl groups from the cofactor *S*-adenosyl-L-methionine (SAM) to arginine residues on chromatin and nonchromatin

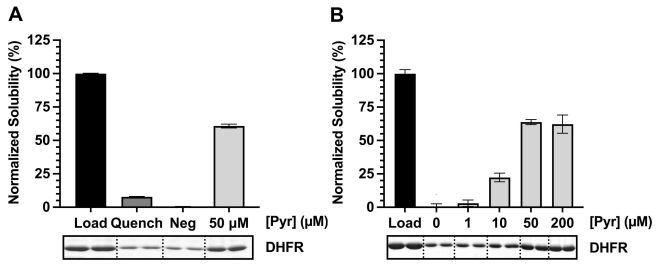

Figure 2. Ligand-dependent ILIRA effect targeting DHFR. A) A comparison in solubility rescue between 50 μM Pyr and 50 μM EPZ015666 (negative control, Neg) with vehicle-only control (1% DMSO for all samples except load), and B) Pyr dose response against 2 μg DHFR (1.7 μM) with vehicle-only control (2% DMSO for all samples except load) are presented as bar graphs along with corresponding gels showing Coomassie-stained DHFR protein bands (n = 2).

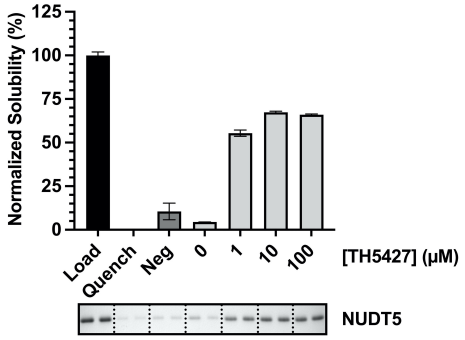

Figure 3. Ligand-dependent ILIRA effect targeting NUDT5. TH5427 dose response against 2 μg NUDT5 (1.6 μM) with vehicle-only control (2% DMSO for all samples except load) and 100 μM EPZ015666 (negative control, Neg) are presented as a bar graph along with the corresponding gel showing Coomassie-stained NUDT5 protein bands (n = 2).

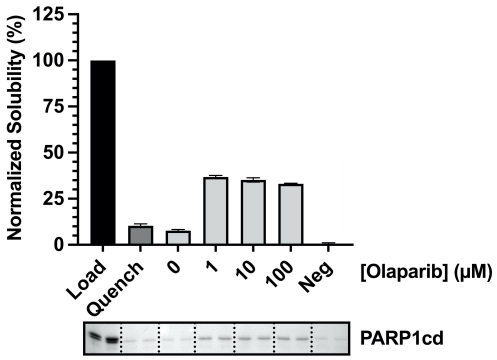

Figure 4. Ligand-dependent ILIRA effect targeting PARP1cd. Olaparib dose response against 2 μg PARP1cd (0.92 μM) with vehicle-only control (2% DMSO for all samples except load) and 100 μM Pyr (negative control, Neg) are presented as a bar graph along with the corresponding gel showing Coomassie-stained PARP1cd protein bands (n = 2).

proteins, generating *S*-adenosyl-L-homocysteine (SAH) as a reaction byproduct and cofactor analogue. PRMT1 functions in a variety of cellular pathways including transcription, splicing, translation, DNA damage response, and receptor signaling.[40] Several types of cancer have shown high levels of PRMT1 expression and concomitant methylation activity that correlates with poor patient prognosis, providing a rationale for PRMT1 as an oncogenic drug target.[41,42]

With the idea that cofactor binding contributes to PRMT1 stability, we performed ILIRA with a dose response of increasing SAH up to 100 μM (Figure 5). Our group previously determined the PRMT1 K_I for SAH is in the range of 5–8 μM,[43] which may explain why the solubility rescue occurred above 10 μM.

Alternative ILIRA sample processing

In resolving protein samples by gel electrophoresis, the throughput of ILIRA can be considered comparable to thermal shift assays like PTSA. Since the proteins we chose for this study were purified to homogeneity, we surmised that using the dot blot platform would result in faster sample processing to see soluble proteins, thus eliminating time-consuming electrophoretic protein separation. We used DHFR with Pyr (positive control) and EPZ015666 (negative control) to demonstrate ILIRA with dot blot sample processing. As shown in Figure 6, only samples treated with 50 μM Pyr showed a DHFR solubility rescue relative to the load, whereas the quench, negative control, and vehicle-only control yielded similarly low signals (see Figure S1 for original Coomassie-stained dot blot). The relative quantitation of signals appeared on par with what we determined in quantifying stained bands on a gel (Figure 2).

An advantage to using the dot blot apparatus is that more conditions can be initially screened to include different pH values, salts, and buffers, as well as more replicates processed in parallel for statistical analysis as compared to a gel limited by the number of lanes available. It is important, nevertheless, to consider an appropriate membrane complementary to the target protein's pI to ensure its retention and subsequent detection. Another advantage is that the soluble fraction of a protein with other contaminating proteins spotted on a dot blot can be probed with an antibody specific for the target protein. Too many contaminating proteins, however, may interfere with the salt and buffer quench needed for ILIRA, so its restricted use on purified proteins is recommended.

To improve ILIRA sample processing, we explored the use of a protein-binding dye. We hypothesized that the use of such a dye may simplify the ILIRA sample processing as there would be no need for gel electrophoresis or dot-blotting post-centrifugation. We explored the amenability of ILIRA with NanoOrange, a highly sensitive, merocyanine dye that, upon interaction with proteins in solution, exerts an enhanced fluorescence.[44] NanoOrange can be used to detect as low as 10 ng/mL of protein in solution, whereas traditional protein quantification reagents, such as bicinchoninic acid (BCA) and Bradford, require a 100 to 1000-fold higher protein concentration.[44–46] We repeated the ILIRA assay with DHFR and Pyr to evaluate ILIRA sample processing with NanoOrange (Figure 7 and S2). The addition of Pyr to DHFR resulted in a dose-dependent increase in fluorescence as a consequence of ligand-induced protein stabilization. A statistically significant

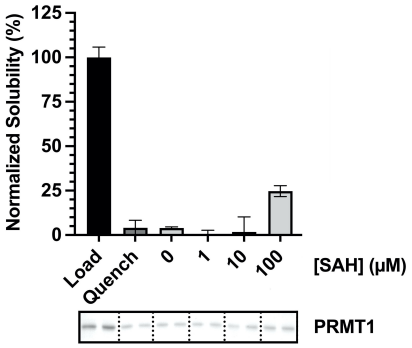

Figure 5. Ligand-dependent ILIRA effect targeting PRMT1. SAH dose response against 2 μg PRMT1 (0.91 μM) up to 100 μM with vehicle-only control (2% DMSO for all samples except load) are presented as a bar graph along with the corresponding gel showing Coomassie-stained PRMT1 protein bands (n = 2).

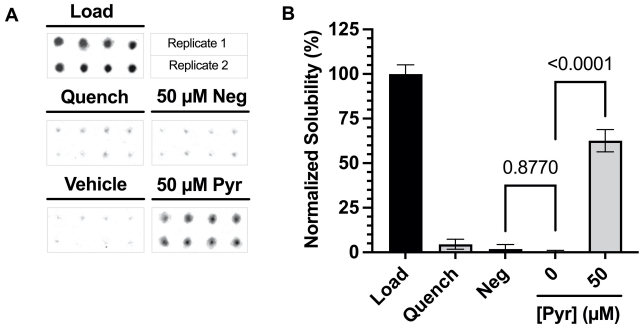

Figure 6. Dot blot ILIRA for DHFR. A) Soluble fractions of treated samples with 2 μg DHFR (1.7 μM) were isolated on P81 filter paper in a dot blot apparatus prior to Coomassie staining and spot densitometry. All samples except load contain 2% DMSO. The negative control (Neg) is 50 μM EPZ015666. ILIRA Replicate 1 (n = 4) was performed on a separate day than ILIRA Replicate 2 (n = 4). B) Densitometric data are presented as a bar graph (n = 8).

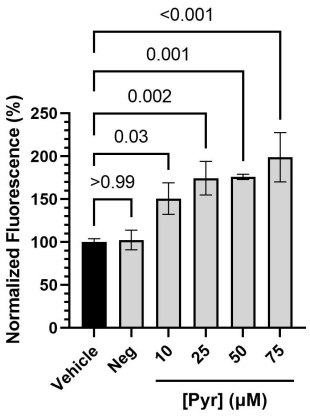

Figure 7. NanoOrange ILIRA for DHFR. Pyr dose response against 10 μM DHFR with vehicle-only control (1% DMSO for all samples) and 75 μM EPZ015666 (negative control, Neg) are presented as a bar graph (n = 3).

difference between the vehicle-only control and samples incubated with Pyr was observed with and without background subtraction when its concentration was at least 25 μM, above its reported IC_{50} value.[25] These data show that NanoOrange can be used as an alternative approach for the relative quantitation of soluble protein present in ILIRA.

NanoOrange protein detection is advantageous over gel electrophoresis and dot blot detection methods since it is a solution-based technique that minimizes sample processing after centrifugation and improves the assay throughput. Use of NanoOrange can involve an additional heating step according to kit instructions to facilitate protein binding and increase fluorescence, but the signal increase has been shown to be relatively small.[47] Nevertheless, the high sensitivity of NanoOrange makes it favorable over alternative protein quantification reagents. Soluble protein detection in solution rather than concentrated in a band (SDS-PAGE) or spot (dot blot) does not, however, concentrate protein signal to the degree that the latter two methods do. To achieve rescue in the NanoOrange-based ILIRA, we had to use a 3-fold higher protein amount (6 μg per sample) in half the volume (10 μM DHFR), which yielded significant differences between treated and untreated samples (Figure 7). In spite of requiring more protein, the increased throughput of NanoOrange-based ILIRA makes it suitable for plate-based screening after sample centrifugation to separate soluble from insoluble fractions.

No spin ILIRA

To further expand the potential application of ILIRA for high-throughput screening, we investigated a solution-based method for the detection of insoluble proteins using two molecular rotor dyes, thus removing the need for the centrifugation step in sample processing. Thioflavin T (ThT) is a benzothiazole dye that binds to β-sheet structures in aggregated proteins, resulting in enhanced fluorescence.[48,49] Proteostat works similarly, and both dyes are commonly used for the detection and quantification of amyloid fibrils in cells.[50–58] We repeated the same ILIRA assay used in Figure 7 for DHFR, but without centrifugation to separate soluble from insoluble proteins, to evaluate ILIRA sample processing with these two aggregation-sensitive dyes. As Pyr was titrated against DHFR in solution, a dose-dependent decrease in fluorescence was observed using ThT compared to the vehicle-only and negative controls (Figure 8A), whereas Proteostat showed a significant and similar decrease compared to vehicle-only and negative controls at all Pyr concentrations (Figure 8B). We observed similar trends even when the sample-matched background signals were subtracted (Figure S3). At lower Pyr concentrations, we were able to detect a dose-dependent decrease trend in fluorescence from Proteostat interacting with aggregated DHFR, but these values were not significant relative to the vehicle-only-control (Figure S4).

Here, we demonstrated that ThT and Proteostat can selectively bind to aggregated DHFR in solution, thereby offering the fastest approach for ILIRA sample processing, with the latter dye showing a more pronounced solubility stress rescue without background subtraction (Figure 8). In the absence of sample centrifugation to separate soluble from insoluble protein fractions, this method allows for aggregated protein detection directly in solution.

In order to detect a statistically significant difference between samples and controls using aggregation-sensitive fluorescent dyes, however, a higher DHFR concentration was required than aforementioned sample processing methods. The DHFR protein stock was concentrated so that the storage buffer concentration would remain low and not affect no spin ILIRA fluorescence measurements. A final DHFR concentration of 30 μM (18 μg per sample) was found in this assay to be optimal with regards to obtaining an adequate and statistically significant signal. In contrast, ILIRA sample detection using Coomassie blue and NanoOrange required lower amounts of protein by 9- and 3-fold, respectively.

No spin ILIRA does require an initial optimization of protein and dye concentrations. ThT protein binding is dependent on

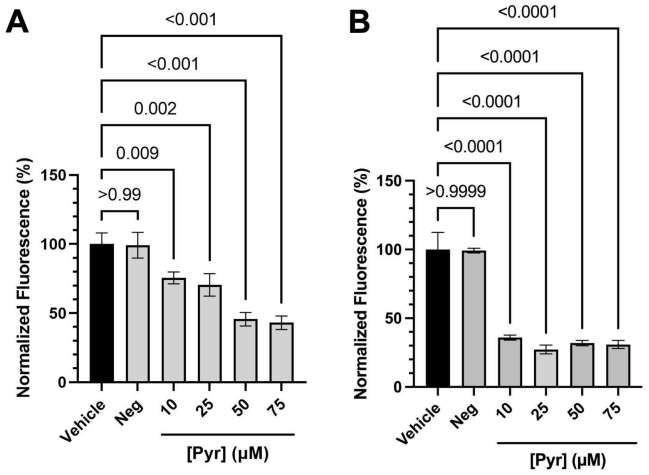

Figure 8. No spin ILIRA for DHFR. (A) ThT and (B) Proteostat were used to detect DHFR aggregation in samples of Pyr dose response with vehicle-only control (1% DMSO for all samples) and 75 μM EPZ015666 (negative control, Neg), presented as bar graphs (n = 3).

protein structure, as well as channel size and shape within aggregates,[48,59,60] and can therefore vary from one protein to the next. Accordingly, varying detection limits have been reported for ThT for different proteins, dipping as low as 10 pM for α-Synuclein aggregates.[49,61] To improve signal for ThT-based ILIRA, we found that a ThT concentration of 50 μM was required to yield full saturation of ThT-binding to aggregated DHFR. At or above 5 μM ThT in PBS, self-fluorescence from the dye has been observed that can lead to a high background signal.[49] At the 50 μM ThT concentration used in our assay, we detected background fluorescence for samples in the absence of protein that did not appear to impact relative values presented in Figure 8A (see Figure S3A).

Proteostat is an alternative molecular rotor dye, offering two important advantages over ThT for no spin ILIRA.[53,54,56] First, Proteostat fluorescence has been shown to be brighter than that of ThT. Second, the spectral excitation and emission for Proteostat is red shifted compared to ThT, indicating that it is less likely to exhibit background fluorescence from UV-active species. Indeed, ThT background fluorescence ranged from 20–60% of the total sample fluorescence, whereas Proteostat background fluorescence proved insignificant, ranging from 3–12% (data not shown). Third, Proteostat appeared to detect rescue of DHFR solubility stress at lower Pyr concentrations than ThT (Figure 8). Taken together, these advantages suggest that Proteostat is more suitable for no spin ILIRA.

The implementation of salt and buffer combinations to destabilize proteins for the purpose of probing for ligand binding represents a significant departure from the established methods of generating protein stress. In this study, we tested the ability of different salt concentrations and types of buffers to elicit a solubility stress in four different proteins overcome by their specific ligands, suggesting that ILIRA may have broad applicability in ligand binding screening for the purpose of identifying enzyme inhibitors. These proteins chosen to demonstrate the proof-of-concept were relatively small, so it is not clear how well the solubility stress and rescue will work with larger, multidomain proteins. The possibility of oligomerization may present another issue for ILIRA. While DHFR is monomeric,[62] NUDT5,[32] PARP1cd,[63,64] and PRMT1[65,66] can form dimeric structures.

ILIRA does require an initial optimization to identify salt and buffer conditions that result in solubility stress. This initial step can serve as an opportunity to address protein concentration needed for the assay, as well as to expand conditions to include different pH values, varied concentrations of different buffers and salts, and a wider temperature range, particularly if initial test conditions do not result in protein aggregation. Even with a small number of variations tested, we were able to arrive at conditions that were destabilizing for all target proteins used in this study, and for which ligand-dependent rescues were possible.

Conclusions

In this proof-of-concept study, we demonstrated multiple methods to adequately quantify soluble or insoluble protein as a means to identify ligands that can rescue protein solubility stress, forming the basis of the ILIRA platform. Using a fluorescent dye like Proteostat to detect protein aggregation in solution greatly improves the efficiency of ILIRA, and can likely be extended to other target engagement assays. These efforts towards improving ILIRA-sample throughput help to establish this method as a screening platform for ligand binding.

Experimental Section

Chemical reagents and materials

Chemicals were purchased as dry powders from commercial suppliers. EPZ015666 (Cayman Chemical, 17285), TH5427 (MedChemExpress, HY-125209 A), Olaparib (Cayman Chemical, 10621) and Pyrimethamine (Cayman Chemical, 16472) were used to make 1.0–7.5-mM stock solutions in 100% DMSO. *S*-adenosyl-L-homocysteine (Millipore Sigma, 1012112) was used to make a 1.0-mM stock solution in 0.5 mM HCl. NanoOrange Protein Quantitation Kit was purchased from Invitrogen (N6666). Thioflavin T (Thermo Fisher Scientific, 211760250) was used to make a 500-μM aqueous stock solution. The 5-μL volume of Proteostat® Detection Reagent (Enzo Life Sciences Inc., ENZ-51023-KP050) was combined with 10X Assay Buffer (Enzo Life Sciences Inc.) to make an aqueous stock solution (200-μL final volume).

DNA Constructs

Human PARP1 cDNA (HG11040-M) was obtained from Sino Biological, and was used as a template to subclone PARP1cd (amino acids 661–1014) into pET-28a(+) at *EcoRI* and *HindIII* sites using the following primers (Integrated DNA Technologies): EcoRI_hPARP1_Primer-F; (5′-AAA AAG AAT TCA CCA AGT CCA AGC TCC CCA AGC C-3′) and HindIII_hPARP1_Primer-R; (5′-AAA AAG CTT TTA CCA CAG GGA GGT CTT AAA ATT GAA TTT CAG-3′). Human Human DHFR (transcript variant 1, mRNA) in pcDNA3.1-C-(k)DYK (NM_000791.4) was obtained from GenScript, and was used as a template to subclone DHFR into pET28a(+) at *NheI* and *BamHI* sites using the following primers (Integrated DNA Technologies): NheI_DHFR_Primer_F: 5′-CTA GCT AGC ATG GTT GGT TCG CTA AAC TG-3′ and BamHI_DHFR_Primer_R: 5′-GCC TAC GGA TCC TTA ATC ATT CTT CTC GTA TAC-3′). The expression vector for recombinant expression of human PRMT1 has previously been described.[66] For cloning applications, DH5α chemically competent *E. coli* cells (Thermo Fisher Scientific, 18265017) were used.

Protein expression and purification

Chemically-competent *E. coli* Arctic Express (Agilent, 230192) were used to recombinantly express PARP1cd and PRMT1 proteins. Cells harbouring expression vectors were grown in LB broth with 50 μg/mL kanamycin (Millipore Sigma, K4000), and induced when the culture reached an OD_{600} of 0.6–0.9 with 1 mM isopropyl β-D-1-thiogalactopyranoside (IPTG) (Millipore Sigma, I6758) at 16 °C for 16 h with 240 rpm shaking. Cells were harvested in a pre-chilled Thermo Fisher Scientific Fiberlite F12-6×500 LEX fixed angle rotor using a Beckman Avanti J-26S series centrifuge at 5000×*g* for 30 min at 4 °C. Pelleted cells were resuspended at 2 mL per gram

cell wet weight in lysis buffer (50 mM HEPES-KOH pH 7.6, 1.0 M NH_4Cl, 10 mM $MgCl_2$, 0.1% Triton X-100, 0.1% Lysozyme (Millipore Sigma, L6876-5G), 25 U/ml DNase I (Millipore Sigma, DN25-10MG), 7.0 mM β-mercaptoethanol (βME), 2.0 mM phenylmethanesulphonylfluoride, EDTA-free Protease Inhibitor Cocktail (Millipore Sigma, 11873580001)) prior to cell lysis using a Branson Sonifier 450 set to 1-s pulses at 50% sonication intensity for ten 30-s intervals. Lysed cells were centrifuged at 35000×*g* for 1 hour at 4 °C in a pre-chilled Thermo Fisher Scientific Fiberlite f21-8x50y fixed angle rotor using a Beckman Avanti J-26S series centrifuge. The supernatant was collected and filtered with a 0.22 μm syringe filter. Using a GE ÄKTA FPLC, filtered supernatant was injected onto a 5 ml HisTrap HP column (Cytiva, 17524701). The column was washed with 7 column volumes of HisTrap wash buffer (50 mM HEPES-KOH, 1 M NH_4Cl, 10 mM $MgCl_2$, 7 mM βME and 10 mM imidazole). Proteins were eluted with HisTrap elution buffer (50 mM HEPES-KOH, 1 M NH_4Cl, 10 mM $MgCl_2$, 7 mM βME and 400 mM imidazole) and collected in 2.5-mL fractions. Fractions corresponding to the highest A_{280} peaks were pooled and re-injected onto a HiLoad Superdex 200 pg preparative size exclusion column (Cytiva, 28989336). The column was washed with SEC buffer (50 mM Tris-Cl pH 7.5 and 100 mM NaCl) until the first sharp peak was observed, at which point 2.5-mL fractions were collected. SEC fractions with the highest A_{280} peaks were pooled and concentrated at 4 °C using 10-kDa MWCO spin filters (Millipore Sigma, UFC9010) at 5000×*g* in an Eppendorf 5810 R centrifuge in protein storage buffer (100 mM HEPES-KOH pH 8.0, 200 mM NaCl, 1 mM DTT, 10% glycerol and 2 mM EDTA). Both proteins were then aliquoted, flash frozen with liquid nitrogen, and stored at −80 °C.

Chemically-competent *E. coli* Rosetta™ (DE3) (Novagen, 70954) was used to recombinantly express DHFR. When the culture reached an OD_{600} of 0.6–0.9, Pyr was added (to a final concentration of 50 μM) and the cells were incubated for 1 h (37 °C, 240 rpm), prior to addition of 1 mM IPTG to induce protein expression (16 °C, 16 h, 150 rpm). Cells were harvested by centrifugation (10000×*g*, 10 min, 4 °C) and cell pellets were frozen at −80 °C. Cell pellets were resuspended in lysis buffer and incubated at 25 °C for 1 h prior to freeze-thaw lysis. Homogenized cell lysates were immersed in liquid nitrogen until frozen, followed by immersion in a 25 °C water bath until fully thawed and repeated for a total of three cycles. Soluble proteins were separated by centrifugation (35000×*g*, 4 °C, 1 h) and filtered through a 0.22 μm low protein binding PVDF membrane (Millex). Clarified lysates were applied to pre-equilibrated Ni-NTA resin (GE healthcare) in wash buffer [50 mM HEPES-KOH pH 7.6, 1 M NH_4Cl, 10 mM $MgCl_2$, 10 mM βME, 10 mM imidazole, 1 mM PMSF] for 1 h at 4 °C. Hexa-histidine tagged DHFR was isolated by applying the lysate-Ni-NTA slurry to a gravity column, discarding the flow-through, washing away non-specifically bound proteins (with 5 CV of wash buffer), and then using stepwise imidazole elution buffers (same composition as wash buffer except for 100–400 mM imidazole) to elute DHFR. Fractions containing DHFR (confirmed by 10% SDS-PAGE) were buffer exchanged in PD10 gravity columns (pre-equilibrated in QHP starting buffer, 20 mM HEPES pH 8.0, 1 mM DTT) and then injected onto a 5 mL HiTrap Q HP column (via AKTA FPLC) also in QHP starting buffer. DHFR was eluted from the Q HP column via a gradient of 0–1 M NaCl (DHFR eluted with 100 mM NaCl as confirmed by SDS-PAGE). Fractions containing purified DHFR were pooled and concentrated in DHFR storage buffer (20 mM HEPES, 300 mM NaCl, 10% glycerol, 20 mM Tris(2-carboxyethyl)phosphine, pH 7.5) using Amicon Ultra 15 mL filters with 10 kDa MWCO (Millipore). DHFR was quantitated using the Bradford protein assay and then aliquoted, flash frozen with liquid nitrogen, and stored at −80 °C.

Protein production and purification of NUDT5 were facilitated by the Protein Science Facility at Karolinska Institutet/SciLifeLab (http://ki.se/psf). The expression clone of NUDT5, provided by Dr. Ann Sofie-Jemth at Karolinska Institutet/SciLifeLab, was transformed into BL21(DE3)T1RpRARE2. An initial overnight culture from a single colony was grown in LB broth with 0.4% glucose at 30 °C and 175 RPM. At 2 OD_{600}, the temperature was set to 18 °C. Induction was performed when cells reached 3 OD_{600}, and protein expression continued overnight until harvested by centrifugation (10 min at 4,500×*g*). IMAC lysis buffer (100 mM HEPES, 500 mM NaCl, 10 mM imidazole, 10% glycerol, 0.5 mM TCEP, pH 8.0) at 1.5 mL buffer per gram cell pellet, and 1 mL per 1.5 L culture of the complete stock solution (1 tablet of Roche Complete EDTA-free protease inhibitor cocktail and 50 μl benzonase nuclease per mL cell resuspension) were added and the cell pellets were resuspended on a shaker table at 4 °C. The resuspended cell pellets were frozen at −80 °C. The frozen cell pellets were briefly thawed in room temperature water and cells were disrupted by pulsed sonication (4-s cycles for 4 min, 80% amplitude). The sonicated lysates were centrifuged (20 min at 49,000×*g*) and the soluble fractions were decanted and filtered through a 0.45-μm filter. Clarified lysate was loaded onto a 5 mL HisTrap HP column (Cytiva, 17524701), washed sequentially in wash buffer (20 mM HEPES, 500 mM NaCl, 10% glycerol, 0.5 mM TCEP, pH 7.5) containing 10 mM and 50 imidazole. NUDT5 was eluted in 20 mM HEPES, 500 mM NaCl, 500 mM imidazole, 10% glycerol, 0.5 mM TCEP, pH 7.5. Eluate was loaded onto a HiLoad 16/60 Superdex 75 (Cytiva) equilibrated in gel filtration buffer (0 mM HEPES, 300 mM NaCl, 10% glycerol, 0.5 mM TCEP, pH 7.5). NUDT5 was concentrated in 10-kDa Vivaspin concentration filters (Vivascience) into its storage buffer (20 mM HEPES, 300 mM NaCl, 10% glycerol, 2.0 mM TCEP, pH 7.5), quantitated by Nanodrop, aliquoted, flash frozen with liquid nitrogen, and stored at −80 °C.

Proteins were quantitated via the Edelhoch method in which we made a 1/10 dilution of target protein in guanidine·HCl (6.6 M) with potassium phosphate buffer (40 mM, pH 6.5).[67] The A_{280} was measured in triplicate on a Thermo Fisher Scientific 2000 1-position Nanodrop spectrophotometer. Expasy's ProtParam tool was utilized to determine the extinction coefficient (ε) of each purified target protein with N-terminal poly-histidine tags (DHFR: 25,440 $M^{-1}cm^{-1}$; PARP1cd: 34,840 $M^{-1}cm^{-1}$; NUDT5: 22,920 $M^{-1}cm^{-1}$; PRMT1: 56,435 $M^{-1}cm^{-1}$).

ILIRA protocol

Buffers were prepared with either 10 mM phosphate buffer (Sodium Phosphate Dibasic (Millipore Sigma, S9762-500G) and Sodium Phosphate Monobasic Monohydrate (Fisher Scientific, ICN19144201)), 10 mM Tris-base (Millipore Sigma, 10708976001), or 10 mM HEPES (Millipore Sigma, H3375), and adjusted to pH 7.4 prior to use. A non-buffered system consisted of ultrapure water alone. NaCl was added to each buffer system to a final concentration of 10 or 100 mM for a total of twelve conditions.

Purified target proteins (2 μg) were added to the twelve conditions in a final volume of 50 μL alongside a 2-μg loading reference for each protein in 10 mM PBS (10 mM phosphate buffer pH 7.6, 100 mM NaCl) with 5X SDS-PAGE sample buffer. Proteins were incubated in the twelve conditions for 30 min at temperatures indicated. Following incubation, the proteins were centrifuged at 20817×*g* at 4 °C for 30 min. The soluble fraction was carefully removed and analyzed by SDS-PAGE. Once destabilizing salt and buffer conditions for individual proteins were identified, the experiment was then repeated with the selected destabilizing condition in the presence of ligands and relevant controls. Following sample processing, the soluble fraction was carefully removed and analyzed by SDS-PAGE gel electrophoresis, dot blot, or NanoOrange fluorescence. ILIRA assays were performed in at least two

independent experiments on different days to repeat results (gels shown are from one experiment).

SDS-PAGE

A 40-μL aliquot of soluble fraction was combined with 5X SDS-PAGE sample buffer prior to being boiled at 95 °C for 5 min. A 10-μL aliquot of each sample was loaded onto a 10% acrylamide SDS-PAGE gel. Gels were stained with a 0.1% (w/v) Coomassie Brilliant Blue G-250 (Thermo Fisher Scientific, 20279) stain solution prior to destaining. Gel images were captured using an Azure Sapphire Biomolecular Imager with Azure's Sapphire Capture Software in live capture mode.

Dot Blot

A 96-well BioRad BioDot Microfiltration Apparatus (BioRad, 1706545) was prepared with P81 cellulose paper (Millipore Sigma, Z753645) and a nitrocellulose (Millipore Sigma, WHA10401114) backing. Under vacuum, 2.0 μl of each sample was pipetted onto the P81 membrane. After 10 seconds, an additional 2.0 μl was added to the same spot for a total of 4.0 μl per well. Following sample addition under house vacuum, the BioDot apparatus was disassembled and filter papers were placed in a 37 °C oven to dry for 15 min. The dried P81 membrane was separated from the nitrocellulose paper, and incubated with Coomassie R-250 (Thermo Fisher Scientific, 20278) stain solution for 15 min. SDS-PAGE destain solution was added to the stained P81 and incubated for 30 min. Post-staining filter paper images were captured using an Azure Sapphire Biomolecular Imager with Azure's Sapphire Capture Software in live capture mode.

Densitometry

Soluble protein levels were quantified using post-imaging densitometry of protein bands or spots. All data collected were in the form of raw pixel intensity; any further data analysis or normalization was performed using raw values. Comparisons were only made between samples of a single gel or dot blot and not between samples in next day replicates. ImageJ 1.53k was used to measure protein band or spot intensity. Average integrated peak areas were normalized with the following equation where X = integrated peak area, Range = integrated peak area between maximum and minimum points in data set and Range Min = smallest integrated peak area in data set:

$$Norm.\ Avg. = \left(\frac{X - Range\ Min}{Range}\right)(100)$$

Like all quantitative methodologies, variance observed between ILIRA densitometry duplicates was present in both SDS-PAGE and dot blot methods. Dot blots generally produced replicates with smaller variance (standard deviation ranging from 1.1–6.6%) compared to the SDS-PAGE gels (standard deviation ranging from 0.3–10.8%).

NanoOrange

In a total volume of 25 μL, 10 μM DHFR in water was incubated in the presence of Pyr and controls at room temperature for 30 min with agitation. The samples were centrifuged at 20,817×*g* for 30 min at 4 °C and 5 μL of the soluble fraction was carefully removed, to which a volume of 245 μL of 1x NanoOrange working solution was added and heated (90 °C, 10 min). Samples were allowed to cool down to room temperature, and 200 μL were aliquoted into a 96-well black polystyrene microplate (Corning #3916) prior to measuring NanoOrange fluorescence on a BioTek Synergy Plate Reader (excitation and emission wavelength of 485 nm and 590 nm, respectively). All measurements were background subtracted with sample-matched controls to account for NanoOrange fluorescence with vehicle and different inhibitor concentrations in the absence of protein.

No spin ILIRA

In a 384-well black polystyrene microplate (Corning #3575), DHFR (18 μg) in water was incubated in the presence of Pyr and controls at room temperature for 30 min with agitation prior to adding 2.5 μL ThT (50-μM final concentration) or 1 μL Proteostat stock solution (1000-fold final dilution); 30 μM DHFR was the final protein concentration in a 25-μL final volume. On a BioTek Synergy Plate Reader ThT fluorescence was measured using 450-nm excitation and 482-nm emission wavelengths, and Proteostat fluoresence was measured using 550-nm excitation and 600-nm emission wavelengths. All measurements were background subtracted with sample-matched controls to account for dye fluorescence with vehicle and different inhibitor concentrations in the absence of protein.

Statistical analysis

Data from Coomassie-stained gels were averaged from same-day duplicates, and duplicate dot blot data were performed in in technical quadruplicate. Experiments with NanoOrange and ThT were performed in triplicate. ILIRA experiments were repeated on two separate days. Experimental data was collected, normalized, and blank-subtracted in Excel before being imported into GraphPad Prism 9.3.1 where analysis was performed using an ordinary one-way ANOVA with Tukey correction for multiple comparisons ($p \leq 0.05$ significance cut-off). All figures were generated using GraphPad Prism 9.3.1 following analysis.

Acknowledgements

We thank the Natural Sciences and Engineering Research Council of Canada (NSERC) (RGPIN-2020-04227 to A.F.; RGPIN-2022-03107 to B.D.G.P.; PGS-D to M.J.R), and the Canadian Institutes of Health Research (PG-461696 to B.D.G.P. and A.F.) for funding support. B.D.G.P is a Michael Smith Health Research BC Scholar. C.C.v.W. was supported by Hendrik Muller and K.F. Hein scholarships. Infrastructure support was provided by an NSERC Research Tools and Instruments Grant (RTI-2021-00633 to A.F.).

Conflict of Interests

The authors declare no conflict of interest.

Data Availability Statement

The data that support the findings of this study are available in the supplementary material of this article.

Keywords: dyes · ligand binding · proteins · solubility stress · target engagement

[1] D. E. Koshland, *Proc. Natl. Acad. Sci. USA* **1958**, *44*, 98–104.
[2] H. Fukada, J. M. Sturtevant, F. A. Quiocho, *J. Biol. Chem.* **1983**, *258*, 13193–13198.
[3] V. Edge, N. M. Allewell, J. M. Sturtevant, *Biochemistry* **1985**, *24*, 5899–5906.
[4] C. Q. Hu, J. M. Sturtevant, *Biochemistry* **1987**, *26*, 178–182.
[5] R. A. Edwards, A. L. Jacobson, R. E. Huber, *Biochemistry* **1990**, *29*, 11001–11008.
[6] G. D. Wiens, T. O'Hare, M. B. Rittenberg, *J. Biol. Chem.* **2001**, *276*, 40933–40939.
[7] E. Papp, P. Csermely, *Handb. Exp. Pharmacol.* **2006**, *172*, 405–416.
[8] R. S. Rajan, K. Tsumoto, M. Tokunaga, H. Tokunaga, Y. Kita, T. Arakawa, *Curr. Med. Chem.* **2011**, *18*, 1–15.
[9] F. H. Niesen, H. Berglund, M. Vedadi, *Nat. Protoc.* **2007**, *2*, 2212–2221.
[10] P. Iliev, D. Hanke, B. D. G. Page, *ChemBioChem* **2022**, *23*, e202200039.
[11] B. Lomenick, R. Hao, N. Jonai, R. M. Chin, M. Aghajan, S. Warburton, J. Wang, R. P. Wu, F. Gomez, J. A. Loo, J. A. Wohlschlegel, T. M. Vondriska, J. Pelletier, H. R. Herschman, J. Clardy, C. F. Clarke, J. Huang, *Proc. Natl. Acad. Sci. USA* **2009**, *106*, 21984–21989.
[12] G. A. Senisterra, B. S. Hong, H.-W. Park, M. Vedadi, *J. Biomol. Screening* **2008**, *13*, 337–342.
[13] S. Boivin, S. Kozak, R. Meijers, *Protein Expression Purif.* **2013**, *91*, 192–206.
[14] K. C. Duong-Ly, S. B. Gabelli, *Methods Enzymol.* **2014**, *541*, 85–94.
[15] Y. Zhang, P. S. Cremer, *Curr. Opin. Chem. Biol.* **2006**, *10*, 658–663.
[16] A. M. Hyde, S. L. Zultanski, J. H. Waldman, Y.-L. Zhong, M. Shevlin, F. Peng, *Org. Process Res. Dev.* **2017**, *21*, 1355–1370.
[17] K. P. Gregory, G. R. Elliott, H. Robertson, A. Kumar, E. J. Wanless, G. B. Webber, V. S. J. Craig, G. G. Andersson, A. J. Page, *Phys. Chem. Chem. Phys.* **2022**, *24*, 12682–12718.
[18] M. Vedadi, F. H. Niesen, A. Allali-Hassani, O. Y. Fedorov, P. J. J. Finerty, G. A. Wasney, R. Yeung, C. Arrowsmith, L. J. Ball, H. Berglund, R. Hui, B. D. Marsden, P. Nordlund, M. Sundstrom, J. Weigelt, A. M. Edwards, *Proc. Natl. Acad. Sci. USA* **2006**, *103*, 15835–15840.
[19] G. A. Senisterra, P. J. F. Jr, *Mol. BioSyst.* **2008**, *5*, 217–223.
[20] E. Ablinger, M. Hellweger, S. Leitgeb, A. Zimmer, *Int. J. Pharmaceut.* **2012**, *436*, 744–752.
[21] F. Bickel, E. M. Herold, A. Signes, S. Romeijn, W. Jiskoot, H. Kiefer, *Eur. J. Pharm. Biopharm.* **2016**, *107*, 310–320.
[22] O.-O. Oyetayo, H. Kiefer, *Pharmaceut. Res.* **2016**, *33*, 1359–1369.
[23] Y. Wang, N. van Oosterwijk, A. M. Ali, A. Adawy, A. L. Anindya, A. S. S. Dömling, M. R. Groves, *Sci. Rep.* **2017**, *7*, 9355.
[24] S. H. Kim, H. J. Yoo, E. J. Park, D. H. Na, *Pharm.* **2022**, *15*, 29.
[25] J. I. Brown, P. Wang, A. Y. L. Wong, B. Petrova, R. Persaud, S. Soukhtehzari, M. L. McDonald, D. Hanke, J. Christensen, P. Iliev, W. Wang, D. K. Everton, K. C. Williams, D. A. Frank, N. Kanarek, B. D. G. Page, *Metabolites* **2023**, *13*, 151.
[26] B. D. G. Page, N. C. K. Valerie, R. H. G. Wright, O. Wallner, R. Isaksson, M. Carter, S. G. Rudd, O. Loseva, A.-S. Jemth, I. Almlöf, J. Font-Mateu, S. Llona-Minguez, P. Baranczewski, F. Jeppsson, E. Homan, H. Almqvist, H. Axelsson, S. Regmi, A.-L. Gustavsson, T. Lundbäck, M. Scobie, K. Strömberg, P. Stenmark, M. Beato, T. Helleday, *Nat. Commun.* **2018**, *9*, 250.
[27] J. Shaw, I. Dale, P. Hemsley, L. Leach, N. Dekki, J. P. Orme, V. Talbot, A. J. Narvaez, M. Bista, D. M. Molina, M. Dabrowski, M. J. Main, D. Gianni, *SLAS Discov.* **2018**, *24*, 121–132.
[28] J. I. Brown, B. D. G. Page, A. Frankel, *Methods* **2020**, *175*, 10–23.
[29] E. E. Abali, N. E. Skacel, H. Celikkaya, Y. Hsieh, *Vit. Horm.* **2008**, *79*, 267–292.
[30] A. Wróbel, K. Arciszewska, D. Maliszewski, D. Drozdowska, *J. Antibiot.* **2020**, *73*, 5–27.
[31] H. S. Kim, S. M. Damo, S.-Y. Lee, D. Wemmer, J. P. Klinman, *Biochemistry* **2005**, *44*, 11428–11439.
[32] M. Zha, C. Zhong, Y. Peng, H. Hu, J. Ding, *J. Mol. Biol.* **2006**, *364*, 1021–1033.
[33] H. Zhang, L.-Q. Zhang, C.-C. Yang, J. Li, X.-Y. Tian, D.-N. Li, J. Cui, J.-P. Cai, *PLoS One* **2021**, *16*, e0245876.
[34] K. E. Pickup, F. Pardow, J. Carbonell-Caballero, A. Lioutas, J. L. Villanueva-Cañas, R. H. G. Wright, M. Beato, *Cancers* **2019**, *11*, 1337.
[35] T. Zhu, J.-Y. Zheng, L.-L. Huang, Y.-H. Wang, D.-F. Yao, H.-B. Dai, *Front. Pharmacol.* **2023**, *14*, 1137151.
[36] J. Hunia, K. Gawalski, A. Szredzka, M. J. Suskiewicz, D. Nowis, *Front. Mol. Biosci.* **2022**, *9*, 1073797.
[37] K. A. Menear, C. Adcock, R. Boulter, X. Cockcroft, L. Copsey, A. Cranston, K. J. Dillon, J. Drzewiecki, S. Garman, S. Gomez, H. Javaid, F. Kerrigan, C. Knights, A. Lau, V. M. Loh, I. T. W. Matthews, S. Moore, M. J. O'Connor, G. C. M. Smith, N. M. B. Martin, *J. Med. Chem.* **2008**, *51*, 6581–6591.
[38] D. V. Ferraris, *J. Med. Chem.* **2010**, *53*, 4561–4584.
[39] I. Goulet, G. Gauvin, S. Boisvenue, J. Côté, *J. Biol. Chem.* **2007**, *282*, 33009–33021.
[40] E. Guccione, S. Richard, *Nat. Rev. Mol. Cell Biol.* **2019**, *20*, 642–657.
[41] J. W. Hwang, Y. Cho, G.-U. Bae, S.-N. Kim, Y. K. Kim, *Exp. Mol. Med.* **2021**, *53*, 788–808.
[42] J. Jarrold, C. C. Davies, *Trends Mol. Med.* **2019**, *25*, 993–1009.
[43] J. I. Brown, T. Koopmans, J. van Strien, N. I. Martin, A. Frankel, *ChemBioChem* **2018**, *19*, 85–99.
[44] L. J. Jones, R. P. Haugland, V. L. Singer, *BioTechniques* **2003**, *34*, 850–861.
[45] M. M. Bradford, *Anal. Biochem.* **1976**, *72*, 248–254.
[46] P. K. Smith, R. I. Krohn, G. T. Hermanson, A. K. Mallia, F. H. Gartner, M. D. Provenzano, E. K. Fujimoto, N. M. Goeke, B. J. Olson, D. C. Klenk, *Anal. Biochem.* **1985**, *150*, 76–85.
[47] S. Silberblatt, R. A. Felder, T. E. Mifflin, *J. Lab. Autom.* **2001**, *6*, 83–88.
[48] M. R. H. Krebs, E. H. C. Bromley, A. M. Donald, *J. Struct. Biol.* **2005**, *149*, 30–37.
[49] C. Xue, T. Y. Lin, D. Chang, Z. Guo, *Roy. Soc. Open Sci.* **2016**, *4*, 160696.
[50] H. Naiki, K. Higuchi, M. Hosokawa, T. Takeda, *Anal. Biochem.* **1989**, *177*, 244–249.
[51] H. LeVine, *Methods Enzymol.* **1999**, *309*, 274–284.
[52] E. Hellstrand, B. Boland, D. M. Walsh, S. Linse, *ACS Chem. Neurosci.* **2010**, *1*, 13–18.
[53] D. Shen, J. Coleman, E. Chan, T. P. Nicholson, L. Dai, P. W. Sheppard, W. F. Patton, *Cell Biochem. Biophys.* **2011**, *60*, 173–185.
[54] S. Navarro, S. Ventura, *Biotechnol. J.* **2014**, *9*, 1259–1266.
[55] S. Navarro, A. Carija, D. Muñoz-Torrero, S. Ventura, *Eur. J. Med. Chem.* **2016**, *121*, 785–792.
[56] S. Oshinbolu, R. Shah, G. Finka, M. Molloy, M. Uden, D. G. Bracewell, *J. Chem. Technol. Biotechnol.* **2018**, *93*, 909–917.
[57] S. Ventura, S. Navarro, *Methods Mol. Biol.* **2018**, *1873*, 195–212.
[58] L. Lesire, L. Chaput, P. C. D. Casas, F. Rousseau, C. Piveteau, J. Dumont, D. Pointu, B. Déprez, F. Leroux, *SLAS Discov.* **2020**, *25*, 783–791.
[59] M. Groenning, L. Olsen, M. van de Weert, J. M. Flink, S. Frokjaer, F. S. Jørgensen, *J. Struct. Biol.* **2007**, *158*, 358–369.
[60] A. Hawe, M. Sutter, W. Jiskoot, *Pharm. Res.* **2008**, *25*, 1487–1499.
[61] C. G. Taylor, G. Meisl, M. H. Horrocks, H. Zetterberg, T. P. J. Knowles, D. Klenerman, *Anal. Chem.* **2018**, *90*, 10385–10393.
[62] D. Baccanari, A. Phillips, S. Smith, D. Sinski, J. Burchall, *Biochemistry* **1975**, *14*, 5267–5273.
[63] H. Mendoza-Alvarez, R. Alvarez-Gonzalez, *J. Biol. Chem.* **1993**, *268*, 22575–22580.
[64] H. Mendoza-Alvarez, R. Alvarez-Gonzalez, *J. Mol. Biol.* **2004**, *336*, 105–114.
[65] X. Zhang, X. Cheng, *Structure* **2003**, *11*, 509–520.
[66] D. Thomas, T. M. Lakowski, M. L. Pak, J. J. Kim, A. Frankel, *Protein Sci.* **2010**, *19*, 2141–2151.
[67] H. Edelhoch, *Biochemistry* **1967**, *6*, 1948–1954.

Manuscript received: November 13, 2023
Revised manuscript received: January 24, 2024
Accepted manuscript online: January 24, 2024
Version of record online: February 12, 2024